



Green and facile synthesis of nickel oxide-porous carbon composite as improved electrochemical electrodes for supercapacitor application from banana peel waste

Sherief A. Al Kiey^{1,2} · Mohamed S. Hasanin³

Received: 6 May 2021 / Accepted: 29 June 2021 / Published online: 8 July 2021

© The Author(s), under exclusive licence to Springer-Verlag GmbH Germany, part of Springer Nature 2021

Abstract

Lithium-ion batteries and supercapacitors are examples of energy storage technologies that have a lot of promise in a variety of applications. Herein, NiO-porous carbon composites were prepared by a green and cost-effective facile synthesis route from banana peel waste materials. The surface morphology and chemical composition of the NiO-porous carbon composite were investigated using a scanning electron microscope (SEM) and energy dispersive x-ray analysis (EDX). The prepared samples were also described through Fourier transform infrared (FTIR) spectroscopy, x-ray powder diffraction (XRD), thermal gravimetric analysis (TGA), and surface area measurements. The electrochemical behavior of prepared materials was studied by cyclic voltammetry (CV), galvanostatic charge-discharge, and electrochemical impedance (EIS) to test their applicable suitability as supercapacitor electrode. PC-NiO (3) composite exhibits a remarkable specific capacitance of 811 F/g at a current density of 1 A/g. The specific capacitance of PC-NiO (3) is 5.3 times more than that of PC material at 1.0 A/g. Furthermore, the PC-NiO (3) composite material still exhibits a specific capacitance of 780 F/g at 5.0 A/g, high rate capability of 84.55% retention at a high current density of 10.0 A/g and superior cycle stability at 1000 cycles. Based on its high specific capacitance, the NiO-porous carbon nanocomposite is one of the most promising electrode materials for supercapacitors, according to the above results.

Keywords Banana peel waste · Porous carbon · Nickel oxide · Cyclic voltammetry · Electrochemical impedance spectroscopy

Introduction

Today, the global energy shortage, especially in most developed parts of the world, seems to be a major issue (Karaman 2021; Lashkenari et al. 2021; Shalan et al. 2020; Sharmoukh et al. 2020). The depletion of fossil resources and climate change caused by large-scale burning of fossil fuels are two of the main reasons for this growing interest (Abdelhameed

et al. 2021). As a consequence, the development of renewable energy and alternative fuels is a promising solution to the problem. The key to lowering storage unit costs is to boost energy storage technologies with greater stability, capacity, and energy density, as well as lower post-maintenance costs (Karaman et al. 2020; Karaman et al. 2021). Supercapacitors (SCs) or electrochemical capacitors are two potential storage systems that are compatible with most renewable energy sources (ECs). Thanks to their high power density and long cycle life, supercapacitors have gained considerable attention for several years compared to secondary batteries (Kötz and Carlen 2000; Miller and Simon 2008; Service RF 2006; Simon and Gogotsi 2010; Wang et al. 2012). Such promising features enable SCs to be potentially applicable in vehicles, portable electronics, memory backup systems, and other electronic industries (Conway n.d., Zeng et al. 2016). However, they have lower density of energy and cycle stability. As a response, the effort has based on increasing energy density while maintaining excellent cycling capability as a means of providing a better energy storage system.

Responsible Editor: Weiming Zhang

✉ Sherief A. Al Kiey
sheriefalkiey@yahoo.com

¹ Electrochemistry and Corrosion Laboratory, National Research Centre, Dokki, Cairo 12622, Egypt

² Material Engineering Lab., Central Network Laboratories, National Research Centre, Dokki, Cairo 12622, Egypt

³ Cellulose and Paper Department, National Research Centre, Dokki, Cairo 12622, Egypt

Energy storage in SCs typically includes two pathways based on energy storage mechanisms, namely, non-faradic and faradic reactions. Electrical double-layer capacitors (EDLCs) have a non-faradic reaction in which there is an electrostatic separation of electrical and ionic charges between the interface of the electrode and the electrolyte. Not only does this electrostatic charge storage system ensure quick energy uptake and transfer, but it also prohibits electrode materials from expanding. This provides the EDLCs with unique power output and a very long cyclic lifetime. Activated carbon materials and conducting polymers in organic electrolytes typically show this behavior (Abdelhameed et al. 2021; Huang et al. 2014; Nyholm et al. 2011; Wei and Yushin 2012), while transition metal oxide materials exhibit faradic reactions involving reduction-oxidation (Redox) reactions with non-rectangular voltammogram and non-linear charge-discharge curves. The exception of a few materials, such as MnO_2 and RuO_2 , which share similar characteristics with neutral electrolyte EDLC materials and are commonly referred to as pseudo-capacitive materials (Wang et al. 2015; Wei et al. 2011). Ruthenium oxide, in particular, has outstanding electrochemical characteristics. Owing to the high price and toxicity of ruthenium oxide, other metal oxides have been studied (Warren et al. 2015; Wu et al. 2010). For its high surface area, high specific capacitance, low cost, and ability to manifest a variety of morphologies, nickel oxide (NiO) has been commonly used for supercapacitors (Cao et al. 2014; Du et al. 2014; Moradlou et al. 2018; Wang et al. 2014). Pure NiO, however, frequently suffers from poor conductivity and limited electrochemical stability, rendering it undesirable for large supercapacitors (Chen et al. 2018; Gawali et al. 2016). Several methods have been successfully intended to address these limitations and enhance the electrochemical efficiency of pseudo-capacitive materials.

EDLC's most extensively utilized electrode material was activated carbon, which was typically made from shells of coal, wood, and coconut. The synthesis of activated carbons from various materials has been studied in recent years by researchers. Researchers have researched in recent years the manufacture of activated carbons from different materials. Based on porous activated carbon, Wang et al. identified cationic starch as a supercapacitor (Wang et al. 2008), and Zhao et al. reported that a supercapacitor electrode composed of activated carbon based on potato starch could also be used (Zhao et al. 2009). Most activated carbons, however, were still made from coal, a resource for non-renewable depletion. The activated carbon sources, with the exception of coal, were mostly plants and crops, but these were food, so it would be a problem. Due to the material's availability and low cost, agricultural waste-based biomass material has gained considerable significance as a precursor material for preparing carbon-based energy storage devices. Carbon electrodes obtained from biomass are an effective alternative because they

have a large specific surface area and excellent electrical conductivity, making them a good candidate for energy storage applications (Ferrero et al. 2015). First, biomass refers to animal and plant-based materials or by-products that can behave as a prospective energy source. Carbohydrates, lignin, starch, protein, and lipids constitute biomass; these components vary depending on the geographical situation and source (Saidur et al. 2011). Biomass contains high levels of carbon, hydrogen, oxygen, and nitrogen, as well as traces of chlorine and sulfur, according to preliminary and final reports. In comparison to other electrode materials for energy and environmental applications, biomass-derived carbon has many significant advantages: (a) abundant and inexpensive availability, (b) eco-friendly in situ nanoporous structure formation, and (d) processing versatility. They can, however, have a variety of chemical functions, making them an excellent applicant for a variety of morphologies in carbon material design (Thomas et al. 2019). Numerous studies have focused on using cheap sources of biomass waste, including banana fibers, to generate useful energy storage materials of high quality for SCs. V. Subramanian et al. (Subramanian et al. 2007), for instance, synthesized activated carbon with increased porosity from agriculture banana fibers using KOH and ZnCl_2 as triggering agents. In 1 M Na_2SO_4 , the material was tested in a possible 1 V window, recording a specific capacitance of 74 F/g obtained. Unfortunately, the activation process affects the carbon yield as well as the use of corrosive materials is not environmentally friendly.

Due to the benefits of double-layer capacitance and pseudo-capacitance, nickel oxide/carbon composite electrodes have been investigated. Katarzyna Lota et al. investigated nickel oxide/carbon composites made by chemical precipitation of nickel hydroxide on active carbon and calcination at 300 °C in air. Nickel oxide, activated carbon, and composite NiO/AC capacitance values ranged from 11 to 90 F/g (Lota et al. 2011). Abioye et al. employed physical activation of the oil palm using microwave to shape nanocomposite material at different temperatures for an electroless plating technique; recording the specific capacitance was 411.52 F/g at 300 °C (Abioye et al. 2017). The high specific capacitance of composite electroactive materials made of nickel oxide and porous carbon, on the other hand, has not been studied.

Therefore, we propose that porous carbon be synthesized from banana waste doped with NiO composites. The current study uses a low-cost, environmentally friendly synthesis method to create porous nanostructured carbon material from non-activated material. The previously activated materials usually use harmful corrosive acids, e.g., phosphoric, nitric, hydrochloric, sulfuric acids. The activation of banana peels in situ is a new technique. The supercapacitor electrodes made from porous carbon-doped nickel oxide electrodes were tested. To test their suitability as supercapacitor electrodes, the electrodes were characterized using electron microscope

(SEM), FTIR, x-ray powder diffraction (XRD), surface area measurements, thermal analysis (TGA, DTG), and electrochemical measurements.

Materials and methods

Materials

From local juice shops, banana peel waste (BPW) was collected. The bright BPW with no disease signs were chosen and thoroughly washed with distilled water. Nickel acetate was purchased in analysis grade from Modern Lab Co, India, with no purification needed. Polyvinylidene fluoride PVDF and N-methylpyrrolidone (NMP) were analytical reagents and were purchased from Alfa Aesar. Nickel foam was supplied by Shanghai Hongxiang Plant. De-ionized water is used to prepare a solution of potassium hydroxide. All materials were used as received without further purification.

Methods

Carbonization of banana peel waste

Grinded BPW was subject to carbonization process at 700 °C under N₂ for 2 h with heating rate 10 °C for min without activation in a muffle. The control sample and treated samples with nickel acetate (1, 3, and 5% (w/w)) were carbonized with same conditions.

Material characterization

Fourier transform infrared (FTIR) spectroscopy (Spectrum Two IR Spectrometer - PerkinElmer, Inc., Shelton, USA) investigated the structural shift. The surface morphology of the composite samples prepared were characterized by field emission scanning electron microscopy (SEM, Quanta FEG 250, FEI) connected to the EDX Unit (energy dispersive x-ray analysis). The SEM sample, a thin layer of Au, was coated with a sputtering coating unit on the sample. Composite micrographs using FESEM were analyzed with Gwyddion 2.45 software to investigate the roughness of the composite [27]. For each sample, 3D micrographs were obtained and the resolution of the micrographs was set. Finally, the parameters of roughness were measured in nm using the same program. Dynamic light scattering (DLS) measurements of the distribution of particle size and zeta potential of the prepared samples were calculated using the Nicomp™ 380 ZLS size analyzer from the USA. Laser light scattering was used at 170° for particle size detection, with the zeta potential measured at 18°. Using the SDT Q600 USA thermal analyzer, thermogravimetric analysis (TGA and DTGA) of composites was carried out in the nitrogen atmosphere with heating rate of 10

°C/min. The Quantachrome Nova-1000 method was used to analyze the sample's N₂ adsorption and desorption isotherms at 77 K temperature. The pore size of the samples was measured and analyzed using the Brunauer-Emmett-Teller (BET) equation. The sum of nitrogen adsorbed at a relative pressure (P/P₀) of 0.97 was used to measure the basic surface areas and pore volumes of nitrogen adsorption desorption isotherms determined by a surface area analyzer.

Electrode preparation

To cast the active electrode material, commercially accessible Ni foam has been used as a current collector. The working electrode was washed with a 1 M HCl solution, DI water, and absolute ethanol for 10 min each under ultrasonication to remove the surface oxide layer before being drop-casted on the Ni foam (2.5 × 1 cm²) and then dried at 80 °C for 3 h. Subsequently, a weight ratio of 80:10:10 was used to disperse a mixture of PC and PC-NiO samples (active material), polyvinylidene fluoride PVDF (binder), and carbon black (conductive material) in 0.5 mL of N-methylpyrrolidone (NMP) as a solvent. The slurry was drop-cast onto the cleaned Ni foam over a working area of 1.5 × 1 cm² and dried at 80 °C overnight in a drying oven.

Electrochemical measurements

In a three-electrode configuration, electrochemical measurements were performed using a Voltalab 40 (France) electrochemical workstation. As shown in Fig. 1, electrochemical measurements were carried out with Ag/AgCl, a Pt wire, and the coated Ni foam as guide, counter, and working electrodes, respectively, and 6 M KOH aqueous solution as the active electrolyte. To investigate the electrochemical performance of the prepared samples, cyclic voltammetry (CV) and galvanostatic CD (GCD) curves were obtained, as well as electrochemical impedance spectroscopy (EIS) in the frequency range of 001 Hz to 100 kHz with an AC amplitude of 5 mV. The CV characteristic and galvanostatic charge/discharge output were measured using a voltage range of 0.0–0.5 V.

Results and discussion

Physical characterization of PCs

Field emission scanning electron microscopy FESEM analyzed the surface morphology of synthesized porous carbon PC and PC/NiO composites (Fig. 2). As indicated in Fig. 2, PCs and composites have a three-dimensional porous structure with cavities and pores, and the average pore size is less than 500 nm, which allows the electrolyte to be moved easily.

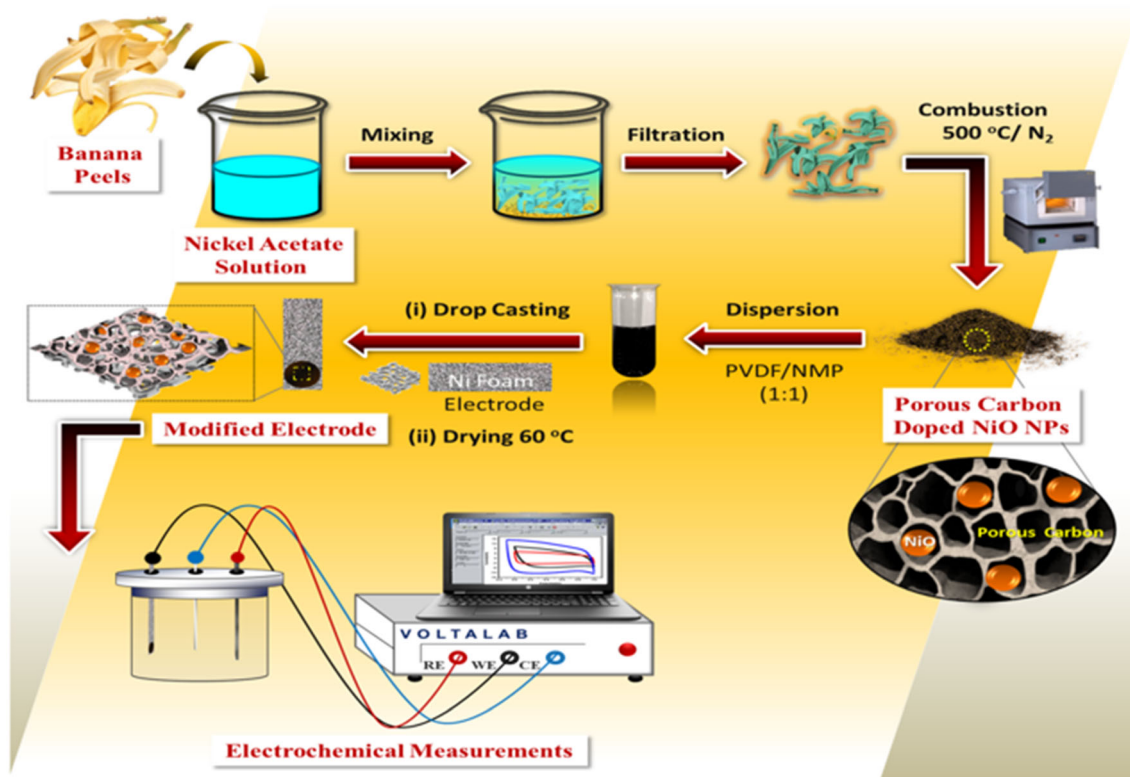


Fig. 1 Schematic illustrations of synthesized electrode materials utilized in supercapacitor application

The EDX study indicated that silicon, phosphorus, calcium, carbon, and oxygen are the main components of porous carbon. The observed calcium content of the carbonaceous raw material is due to its normal occurrence. The prepared PC is enriched with oxygen species that would strengthen Ni/or NiO’s attachment during impregnation to the carbon surface. EDX research has characterized the chemical composition of NiO/PC powders. In addition to oxygen, carbon and nickel occurred in the specimens. In the as-prepared sample (Ni/PC), EDX analysis showed a high carbon to Ni atomic ratio approaching

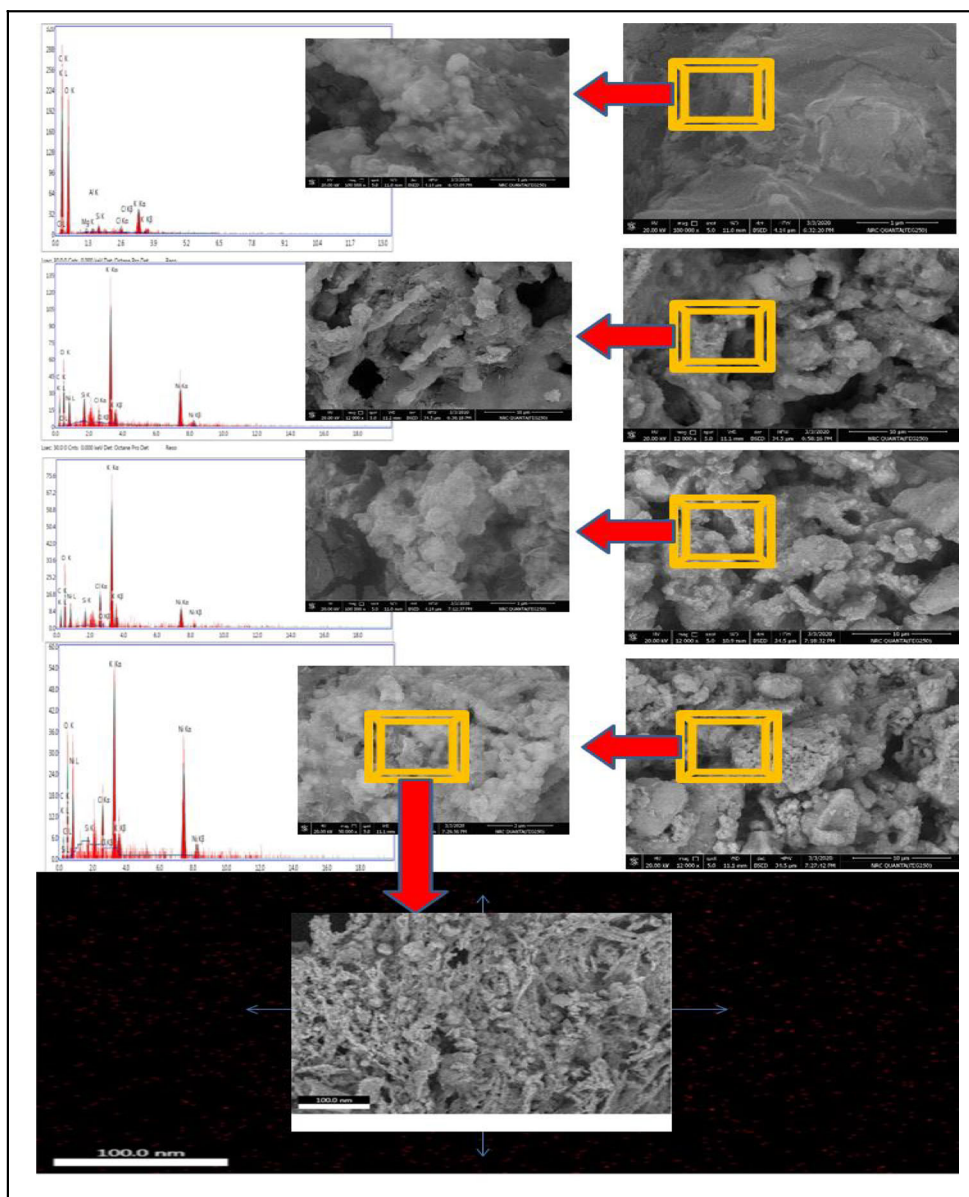
The behavior of surface roughness has been performed to make more identifications to the surface (Aly and Ahmed 2021; El-Kader et al. 2021) as shown in Fig. 3 and the roughness data are presented in Table 1. It could be noticed that the average roughness (R_a) of the PC was 105.624 nm and after the doping with NiO, this value has been raised to 183.201 nm for Pc-NiO₃ which confirms that doping of PC with NiO enhancing surface roughness. Simultaneously, the root mean square roughness (R_q) exhibit the same pattern as R_a , rising from 158.852 nm for PC to 204.603 nm for PC-doped NiO₃. It has been observed that doping PC with more NiO results in a large increase in PC surface roughness.

For further examination, FTIR was performed to outline the newly functional groups bearing nanocomposite. It is well known that, the original character of banana peel waste mostly appears in FTIR spectra of prepared PC samples as most

lignocellulosic material carbons. This means that the produced PCs are characteristics with a unique features as well as the carbon properties. Figure 4 illustrates the FTIR spectra of prepared PCs. The bands which characterized the lignocellulose materials are observed at about 3440, 2925, 1630, 1400, and 1135 cm^{-1} which referred to OH stretching vibration, C-H stretching, C=O of carboxylic group, C=C of aromatic rings, and C-O-C stretching, respectively (Abou Hammad et al. 2019; Basta et al. 2019). Moreover, the addition of Ni ions is shown a significant change between native PC and Ni-doped PCs. Hence, the intensity of C=O peaks in the three doped PCs is decreasing with low shift in the low frequency as well as C-H starching peaks. In context, appearing of new peaks around 637 and 426 cm^{-1} which may be corresponds to vibrations of Ni-O bonds (Kayani et al. 2018). In addition, the concentration of Ni ion is affecting the behavior of PCs toward IR spectra. The intensity as well as the position of characteristic peaks which detected in native PCs where effect. The intensity of characteristic peaks is decreased with increase of Ni ions as a result to the interaction of Ni ions with PC active group. In context, the positions of characteristic peaks which appear in native were shifted to lower frequency by the same effect on intensity.

The XDR patterns of PC illustrated the crystallographic ordering profile of each preparation conditions. Figure 5 shows the XRD pattern of as-prepared PC composites. The pristine porous carbon sample showed a characteristic peaks at

Fig. 2 FESEM of (a, b) PC and its corresponding EDX, (c, d) PC/NiO1 and its corresponding EDX, (e, f) PC/NiO2 and its corresponding EDX, (g, h) PC/NiO3 and its corresponding EDX, and (i) mapping of PC/NiO3



24.26 and 42° which attributed to (002) and 101 diffractions

Table 1 Roughness parameters including roughness average (Ra), root mean square roughness (Rq), the maximum height of the roughness (Rt), and maximum roughness valley depth (Rv) of blank and NiO-doped PC

Sample	Roughness average R_a (nm)	Root mean square roughness R_q (nm)	Maximum height of the roughness (Rt)	Maximum roughness valley depth (Rv)
Blank	105.624	158.852	534.975	296.927
PC-NiO1	109.624	178.852	552.975	305.927
PC-NiO2	129.206	188.800	554.979	329.001
PC-NiO3	183.201	204.603	591.481	365.271

(Gomes Ferreira de Paula et al. 2019). These finding peaks are close to petroleum coke with the amorphous nature (Mopoung et al. 2015). In context, the doping of PCs with Ni ion referred significant changes in the doped PC XRD pattern. Moreover, the peaks which characterized crystal planes indicated the formation of phase pure, cubic nickel oxide are observed clear in 37.23, 43.3, 62.90, 75.7, and 79.87° which corresponding to (111), (200), (220), (311), and (222) respectively (JCPDS-780429) (Dharmaraj et al. 2006). Additionally, the patterns of doped PCs emphasized the increase of doped Ni ion percentage which leads to increasing the PC crystallinity.

The surface area and porosity of PC and PC-NiO composites were investigated using BET analysis at 77 K. Figure 6 displays the N₂ adsorption/desorption isotherm and corresponding BJH pore size distribution plot of the synthesized

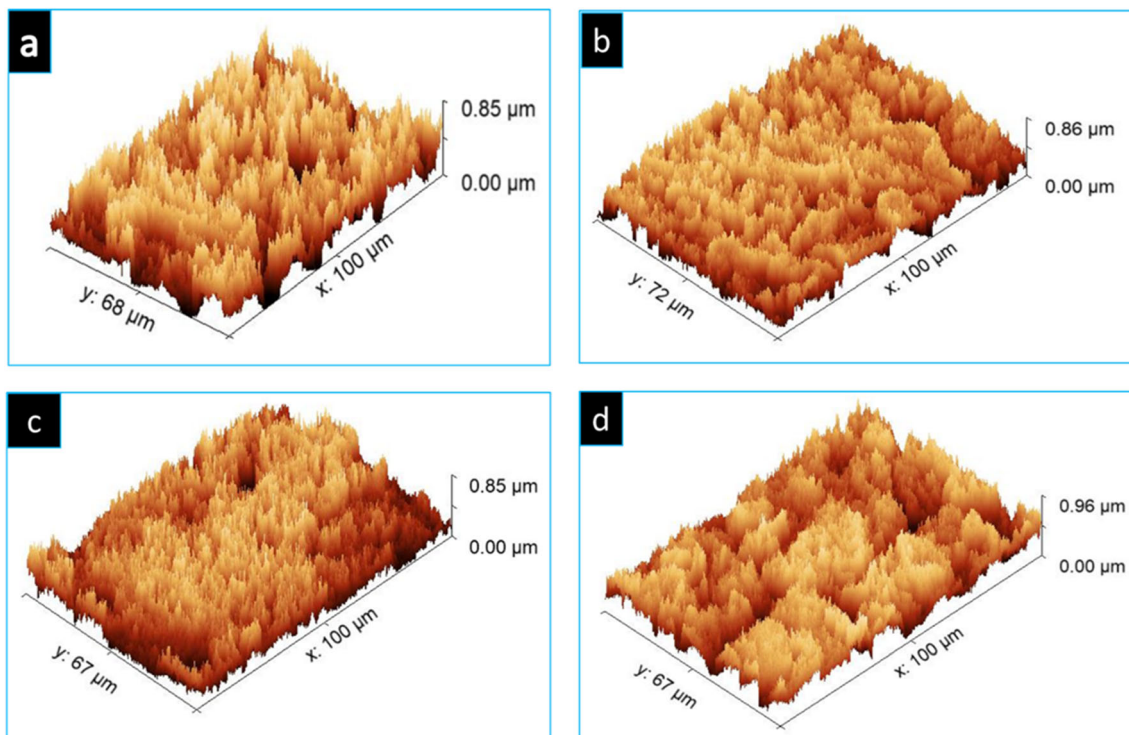


Fig. 3 Surface roughness behavior of (a) PC, (b) PC-NiO1, (c) PC-NiO2, and (d) PC-NiO3

samples. The isotherm graph shapes are unique for each surface behavior. The PC sample isotherm graph types can be categorized as typical type IV(a) isotherm type with an H_3 hysteresis loop at the relative pressure, suggesting the presence of mesopores in the sample according to the following IUPAC classification according to Thommes et al. (Thommes et al. 2015).

The calculated BET-specific surface areas of the PC, PC/NiO (1), PC/NiO (2), and PC/NiO (3) are 465, 510, 691, and 1187 $m^2 g^{-1}$, respectively, as shown in Table 2 which means that the addition of NiO to PC increased the surface area and PC/NiO (3) has the greatest surface area hence expected to deliver higher capacity than other samples. The average pore diameter and pore volume of the PC, PC/NiO(1), PC/NiO (2),

and PC NiO (3) are 2.72, 2.79, 2.97, and 8.28 nm and 0.637, 0.695, 1.768, and 2.857 $cm^3 g^{-1}$, respectively. The comparable specific surface area of prepared samples leads to increased ion accessibility at the electrode/electrolyte interface. PC/NiO (3)'s unique surface area and pore structure improve the Faradaic redox couple operations, resulting in the electrode material's superior electrochemical performance in supercapacitor applications.

Moreover, the volume adsorption axis in the prepared PCs show a significant change where the gas adsorbed is referring

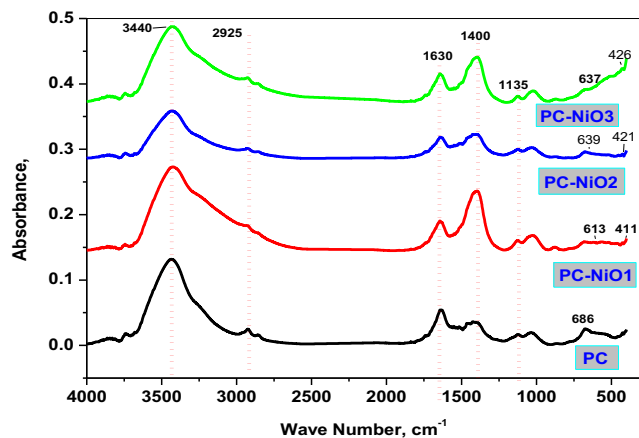


Fig. 4 FTIR of prepared porous carbon-doped nickel oxide

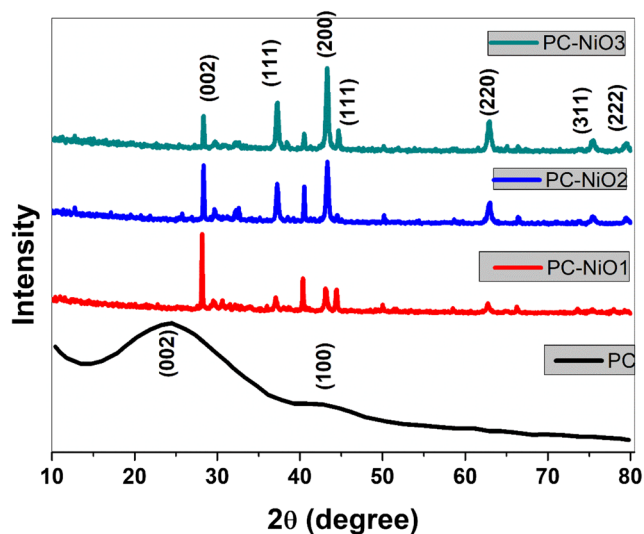


Fig. 5 XRD patterns of (a) PC, (b) PC-NiO1, (c) PC-NiO2, and (d) PC-NiO3

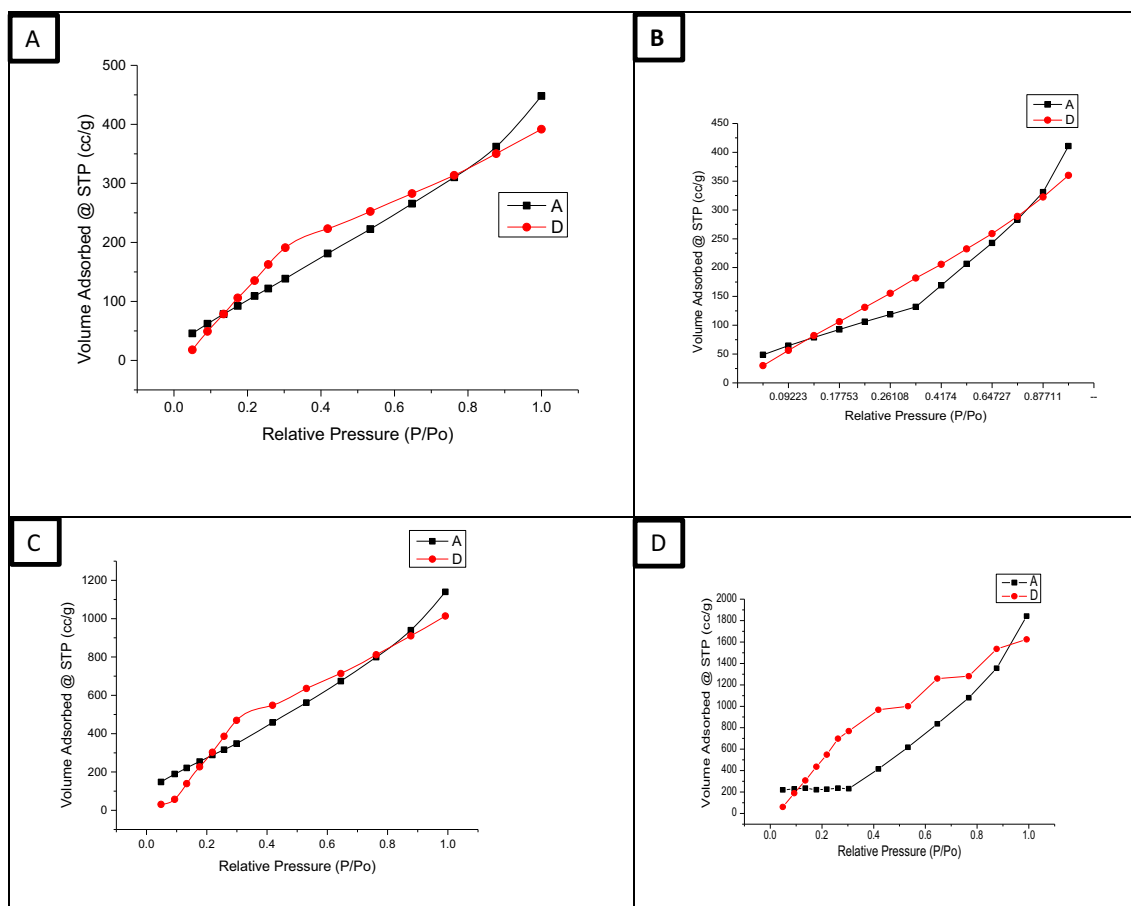


Fig. 6 Nitrogen adsorption-desorption isotherm of the (A) PC, (B) PC-NiO(1), (C) PC-NiO(2), and (D) PC-NiO(3)

to the surface area as well as porosity. The blank PC and doped sample with 1% Ni are more closed. On the other hand, the samples 3% and 5% showing an improvement in adsorbed gas volume. These results are in agreement with the surface results in Table 1 which offered that the surface area of sample 5% Ni is duplicated of blank sample and 1, 3% Ni-doped PC. In addition, the pore volume of sample 5% is duplicated of sample 3% as well as fourfold of blank PC and 1% Ni-doped PC. In context, the sample 5% clear an increase in mesopore as well as pore diameter is compared with the other PC samples. These results emphasize that the surface structure of blank sample is a heterogeneous pore distribution with amorphous behavior. Hence, the addition of Ni ion leads to increase

of surface homogeneity, poor homogeneity distribution, and crystallinity.

The DLS measurements illustrated informative results about the PC surface charge and particle size distribution and the data are tabulated in Table 3. The zeta value of blank PC (-5.21 mV) is improved with the addition of Ni ion where recorded -139.97 mV. These results mean that the addition of Ni ion enhances the stability of colloidal solution of PC (Kumar and Dixit 2017) as well as increases the PC surface charge. Moreover, the value of zeta in PCs doped with 3% and 5% Ni ion referred to nanoparticle present of Ni ion. In addition, the particle size distribution measurements appear that the particles in PC 5% doping are may in nanoscale with average particle size 389.6 nm. In fact, this value in absolute

Table 2 Surface area and textural parameters of as-prepared samples

Sample code	Carbon yield (C) %	S_{BET} , m^2/g	$C \times S_{\text{BET}}$, m^2/g	$V_{\text{T}(0.95)}$, cm^3/g	$S_{\text{mes(BjH)}}$, cm^3/g	S_{mic} , m^2/g	Pore diameter, nm
PC	55.4	465	25761	0.637	248	117	2.723
PC-NiO 1	62.9	510	32079	0.695	279	123	2.743
PC-NiO 2	71.2	691	49199.2	1.768	332	134	2.978
PC-NiO 3	76.3	1187	90568.1	2.857	1026	187	8.286

Table 3 DLS measurements of prepared composites

	Zeta potential measurements				Particle size measurements	
	Cell current, mA	Av. phase shift, rad/sec	Av. mobility, M.U.	Av. zeta potential, mV	PDI	Average particle size/nm
Blank	2.41	-0.10	-0.36	-5.21	0.176	799.8
PC-NiO 1	1.36	-0.40	-0.82	-11.75	0.404	597.9
PC-NiO 2	1.01	-2.41	-3.0	-43.0	0.406	395.9
PC-NiO 3	1.23	5.76	9.74	-139.97	0.511	389.6

is not nanosized but when we consider the structure of PC as well as the aggregation of particle, this value can be considered as nanosized. Overall the DLS results are confirmed that the prepared PCs are improved in surface charge, stability, and nanosized with an increase of Ni ion addition.

Thermal gravimetric analysis as well as its derivative for prepared PCs is illustrated in Fig. 7. All the tested PC samples are performed with the same thermal behavior. The first peak of degradation is observed around 168 °C. However, the second degradation peak shows a significant difference between the prepared PCs. The native PC sample recorded this peak at 649 °C as sharp. In addition, the PC samples PC-NiO (1) and PC-NiO (2) are recorded, this peak at about 645 °C as flat peaks. On the other hand, the sample PC-NiO (3) showed a change in this peak behavior where the peak was shifted to 677 °C as flat sharp peak. These results emphasize that the Ni oxide molecules are involved in the intermolecular structure of the PC sample and affect their thermal behavior as well as affect the physical characterization. Furthermore, the Ni concentration affects the thermal stability of the prepared PC sample, with the thermal stability increasing in full agreement with the Ni concentration.

Electrochemical performance

In a three-electrode cell with aqueous electrolyte of 6 M KOH, the electrochemical performance of the working electrode were assessed at room temperature. Cyclic voltammetry (CV) and galvanostatic charge-discharge (GCD) experiments were carried out to assess the charge storage efficiency of PC/NiO composite electrodes. Figure 8 compares the CV curves of porous carbon PC, PC/NiO-1, PC/NiO-2, and PC/NiO-3 composite electrodes in the potential window range of 0.0 to 0.5 V at various scan rates of 5, 10, 25, 50, and 100 mV s⁻¹. For all electrodes, pair of well-defined redox peaks (Fig. 8b, c, d) were observed, suggesting that the stored energy mainly derived from faradaic reactions (oxidation and reduction). The possible electrochemical reactions in KOH electrolyte are given below (Lu et al. 2011; Wang et al. 2014).



The oxidation of NiO to NiOOH induced the anodic peak to appear at about 0.3 V, while the reduction of NiOOH to

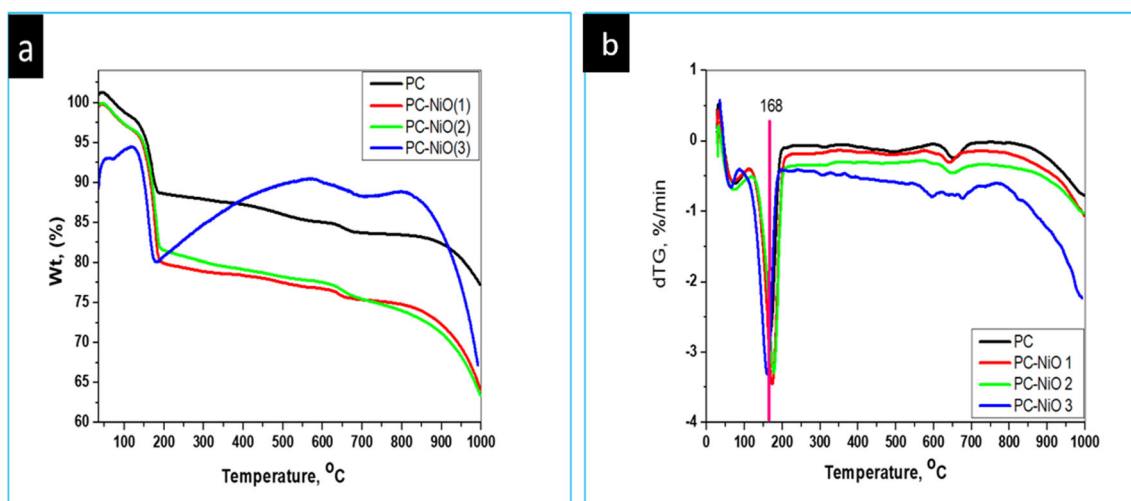


Fig. 7 Thermal gravimetric analysis and its derivatives for the synthesized composites

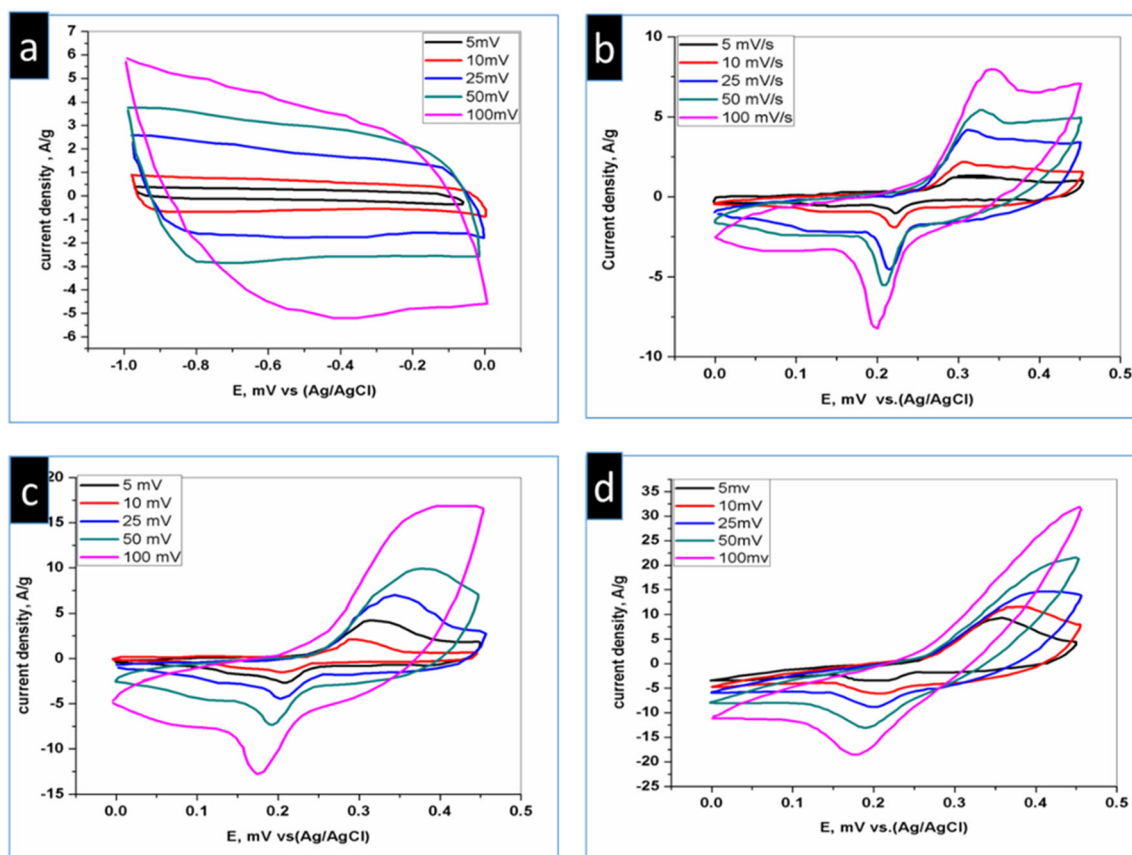


Fig. 8 (a) CV curves of PC electrodes, (b) CV curves of the PC/NiO (1), (c) CV curves of the PC/NiO(2), (d) CV curves of the PC/NiO(3) electrode at different scan rates 25, 50, and 100 mV/s in 6 M KOH solution

NiO induced the cathodic peak to appear at 0.2 V. A faradaic pseudo-capacitance is generated by the presence of nickel oxide, and porous carbon with a high specific area can provide both a broad double-layer capacitance.

The specific capacitance of composite electrodes can thus be increased by combining double-layer capacitance and Faradaic pseudo-capacitance. As the scan rate was increased from 5 to 100 mV s⁻¹, the oxidation peak potential shifted to higher and lower potentials, showing a greater potential distinction between the oxidation and reduction peaks and implying that the redox reaction is reversible. Furthermore, the shapes of the CV curves were well preserved when the possible scan rates ranged from 5 to 100 mV s⁻¹, suggesting the electrodes' excellent rate capability and enhanced mass transport, as well as the structure's uniqueness for fast redox reactions. As the scan rates increased, the samples' specific capacitance decreased. The determined specific capacitances were calculated from CV measurements and revealed that PC-NiO (3) has the highest rate capability as it has the largest current response and integral region of the CV curve among the prepared electrodes, suggesting that it has the highest pseudo-capacitance. This is due to the fact that the samples' crystalline structure, morphology, and BET surface area differ from those of the other samples.

Galvanostatic charge/discharge measurements were also carried out to investigate the electrode performance of the prepared electrode, as shown in Figure 9. The following equation can be used to measure the specific capacitance from the galvanostatic charge-discharge (Lamiel et al. 2017)

$$C_{sp} = \frac{I(\Delta t)}{(\Delta E m)} \quad (2)$$

In this equation, C_{sp} is the specific capacitance, I is the discharge current, Δt is the discharging time, ΔE is the potential window of the electrolyte, and m is the mass of the working material (Lee et al. 2012a).

Figure 9 displays the GCD galvanostatic charge-discharge curves of PC electrodes and PC-NiO composites. Figure 9a shows a triangular shape between 0 and -1.0 V for porous carbon PC electrodes versus Ag/AgCl at different current densities, indicating that PC as electrodes in 6 mole L⁻¹ KOH solution has good Coulombic efficiency and ideal capacitive behavior.

The specific capacitances were calculated at current density 1 A/g for PC, PC-NiO (1), PC-NiO (2), and PC-NiO (3) as 151.52, 493.02, 661.15, and 811.46 F/g, respectively and the

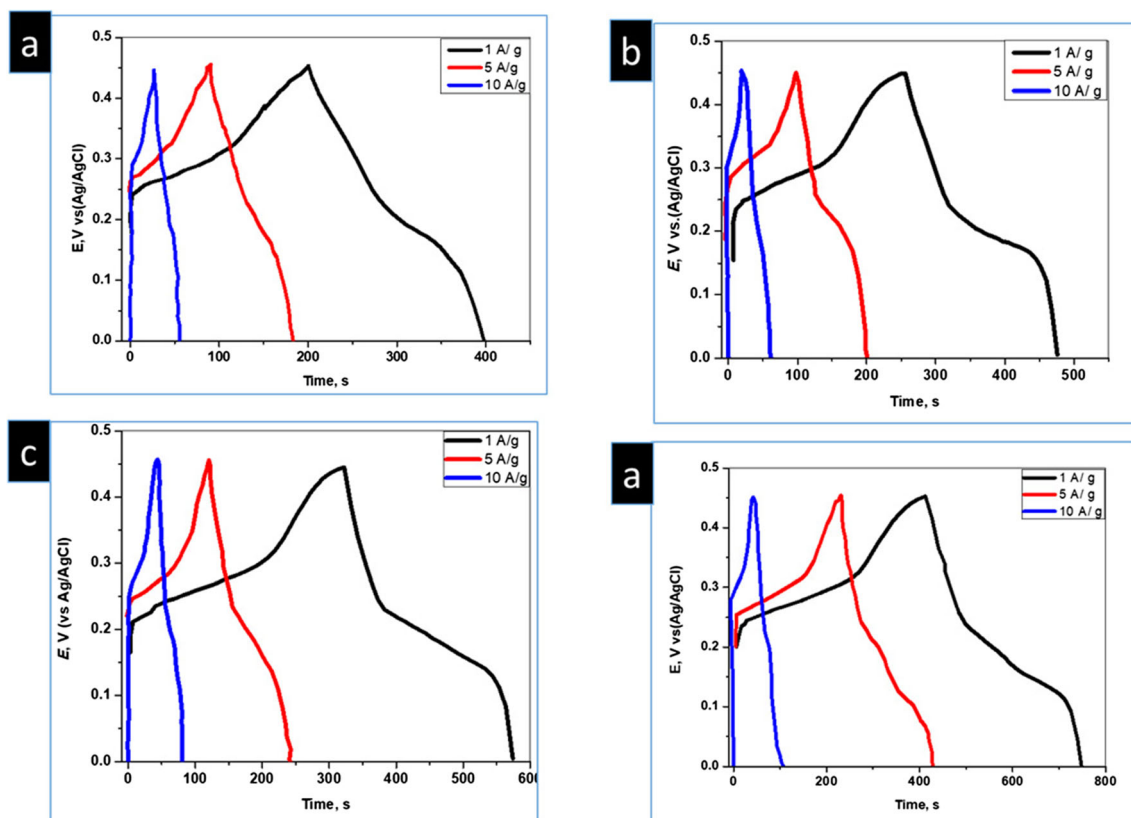


Fig. 9 Galvanostatic charge/discharge of (a) PC, (b) PC-NiO 1, (c) PC-NiO 2, and (d) PC-NiO 3 at various scan rates

results are presented in Table 4. PC-NiO (3) composite maintains the best capacitance when the current density increased than the PC electrodes and other composites. The specific capacitance of PC-NiO (3) is 5.3 times more than that of PC material at 1.0 A/g. Furthermore, the PC-NiO (3) composite material still exhibits a specific capacitance of 471.20 and at 5.0 A/g and 658.72 F/g at a high current density of 10.0 A/g as shown in Fig. 10.

It should be observed that all composite materials prepared have greater capacitance than PCs alone, suggesting that porous carbon is affected by NiO doping. The highest specific capacitance of the PC-NiO(3) composite could be due to the improvement in surface properties relative to the other composite materials in Table 4. In addition, the doping of NiO

particles into porous carbon has a significant effect on the surface properties of the carbon pores. The high specific capacitance was obtained for active materials with high specific surface area and pore distribution that facilitates the diffusion of OH ions by a redox reaction at the electrolyte/active material interface. These findings demonstrate that the introduction

Table 4 Calculation of Specific capacitance (F/g) calculated from galvanostatic charge-discharge measurements for PC, PC/NiO (1), PC/NiO (2), and PC/NiO (3) composites

Current density (A/g)	PC	PC-NiO 1	PC-NiO 2	PC-NiO 3
1	151.52	493.02	661.15	811.46
5	106.47	409.44	572.80	780.80
10	75.48	293.67	471.2	658.723

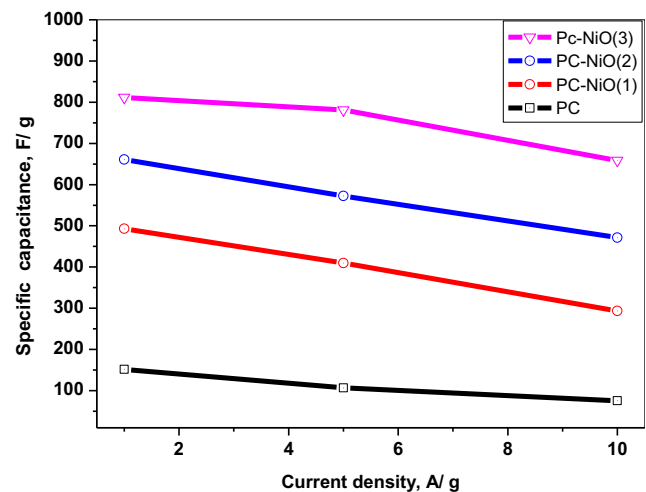


Fig. 10 Relationship for PC and PC-NiO composite materials between specific capacitance and current densities

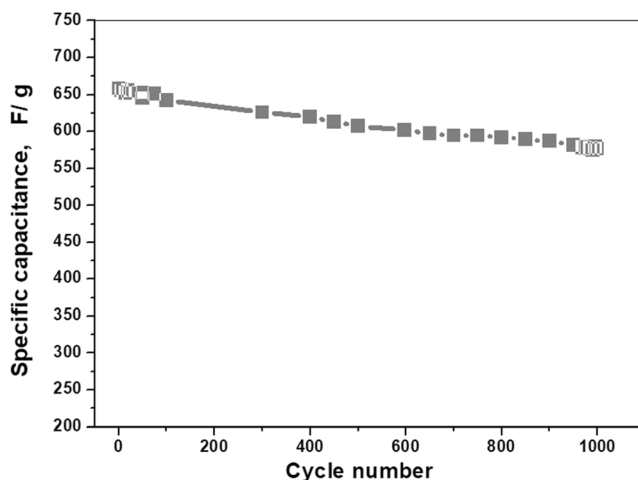


Fig. 12 Cycle test of PC-NiO(3) to 1000 cycles at a 10 A/g current density

of NiO is a powerful way for improved electrochemical properties to be achieved.

EIS (electrochemical impedance spectroscopy) is a useful technique for studying more about the electrochemical properties of PC and PC/NiO composite materials. Figure 11 shows the Nyquist plots for PC and PC/NiO composite electrodes. At a high frequency, the Nyquist plots display a semi-circle with a small radius and an inclined vertical line at a low frequency. A vertical line indicating the degree of electrochemical capacitive characteristics of porous carbon doped with NiO composites, which is a function of OH⁻ ion diffusion at the electrolyte and active material interface (Bao et al. 2009; Lee et al. 2012b). The supercapacitor behaves similarly to an ideal capacitor, as shown by a line that is more perpendicular to the imaginary y-axis. As compared to the other samples, the vertical line of PC-NiO (3) leans more toward the y-axis, indicating that PC-NiO (3) has excellent electrochemical action. The Nyquist plots increase with a nearly 45°

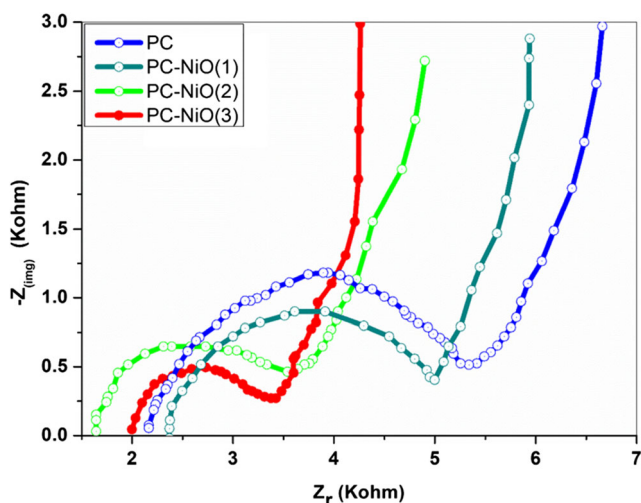


Fig. 11 Nyquist plots of porous carbon and porous carbon doped with different Ni content electrodes in 6 M KOH solution

line in the intermediate-frequency field, corresponding to the characteristic of ion diffusion into the carbon electrodes.

The charge-discharge cycling tests of PC-NiO(3) at a current density of 1 A/g for 1000 cycles are shown in Figure 12. After 1000 cycles, the real capacitance of PC-NiO(3) remained 95.25% of its initial value. The PC/NiO composites are thought to allow easy OH access to the NiO electrode surface, resulting in a high specific capacitance and less degradation during the cycle test.

Conclusion

Porous carbon was prepared by a green and facile synthesis route from banana peel waste materials. This porous carbon-doped nickel oxide. Three-dimensional porous structure with cavities and the average pore size is less than 500 nm was revealed by SEM. The crystallinity of nanocomposite and formation of phase pure, cubic nickel oxide was affirmed via XRD. N₂ adsorption-desorption analysis showed that prepared porous carbon and its composites have a high surface area. A pair of well-defined redox peaks was observed for all electrodes indicating that the stored energy mainly originated from the Faradaic reactions (oxidation and reduction of Ni) ions which demonstrates pseudo-capacitive capacitance behavior based on a fast redox mechanism. PC-NiO(3) composite maintains the best capacitance when the current density increased than the PC electrodes and other composites. The specific capacitance of PC-NiO (3) is 5.3 times more than that of PC material at 1.0 A/g. Furthermore, the PC-NiO(3) composite material still exhibits a specific capacitance of 471.20 and at 5.0 A/g and 658.72 F/g at a high current density of 10 A/g and superior cycle stability at 1000 cycles.

Acknowledgements The authors thank the National Research Centre (NRC) for the technical support.

Availability of data and materials All data and materials are available.

Author contribution S.A. Al Kiey and M.S. Hassenin: Conceptualization, formal analysis, writing — review and editing, project administration, funding acquisition, supervision

Funding The authors thank the National Research Centre (NRC) for the financial support.

Declarations

Ethical approval Not applicable

Consent to participate The authors are consent to participate the article.

Consent to publish The authors are consent to publish the article.

Competing interests The authors declare no competing interests.

References

- Abdelhameed RM, Al Kiey SA, Wassel AR, El-Shahat M (2021) Silver chromate doped Ti-based metal organic framework: synthesis, characterization, and electrochemical and selective photocatalytic reduction properties. *New J Chem* 45:9526–9537
- Abioye AM, Noorden ZA, Ani FN (2017) Synthesis and characterizations of electroless oil palm shell based-activated carbon/nickel oxide nanocomposite electrodes for supercapacitor applications. *Electrochim Acta* 225:493–502
- Abou Hammad A, Abd El-Aziz M, Hasanin M, Kamel S (2019) A novel electromagnetic biodegradable nanocomposite based on cellulose, polyaniline, and cobalt ferrite nanoparticles. *Carbohydr Polym* 216: 54–62
- Aly AA, Ahmed MK (2021) Nanofibers of cellulose acetate containing ZnO nanoparticles/graphene oxide for wound healing applications. *Int J Pharm* 598:120325
- Bao N, Shen L, Wang YHA, Ma J, Mazumdar D, Gupta A (2009) Controlled growth of monodisperse self-supported superparamagnetic nanostructures of spherical and rod-like CoFe₂O₄ nanocrystals. *J Am Chem Soc* 131:12900–12901
- Basta AH, Lotfy VF, Hasanin MS, Trens P, El-Saied H (2019) Efficient treatment of rice byproducts for preparing high-performance activated carbons. *J Clean Prod* 207:284–295
- Cao F, Pan G, Xia X, Tang P, Chen H (2014) Synthesis of hierarchical porous NiO nanotube arrays for supercapacitor application. *J Power Sources* 264:161–167
- Chen J, Peng X, Song L, Zhang L, Liu X, Luo J (2018) Facile synthesis of Al-doped NiO nanosheet arrays for high-performance supercapacitors. *R Soc Open Sci* 5:180842
- Conway BE (n.d.) *Electrochemical supercapacitors: scientific fundamentals and technological applications*. Springer Science & Business Media
- Dharmaraj N, Prabu P, Nagarajan S, Kim CH, Park JH, Kim HY (2006) Synthesis of nickel oxide nanoparticles using nickel acetate and poly(vinyl acetate) precursor. *Mater Sci Eng B* 128:111–114
- Du D, Hu Z, Liu Y, Deng Y, Liu J (2014) Preparation and characterization of flower-like microspheres of nano-NiO as electrode material for supercapacitor. *J Alloys Compd* 589:82–87
- El-Kader MFHA, Ahmed MK, Elabbasy MT, Afifi M, Menazea AA (2021) Morphological, ultrasonic mechanical and biological properties of hydroxyapatite layers deposited by pulsed laser deposition on alumina substrates. *Surf Coat Technol* 409:126861
- Ferrero G, Fuertes A, Sevilla M (2015) From soybean residue to advanced supercapacitors. *Sci Rep* 5:16618
- Gawali SR, Dubal DP, Deonikar VG, Patil SS, Patil SD, Gomez-Romero P, Patil DR, Pant J (2016) Asymmetric supercapacitor based on nanostructured Ce-doped NiO (Ce: NiO) as positive and reduced graphene oxide (rGO) as negative electrode. *ChemistrySelect* 1: 3471–3478
- Gomes Ferreira de Paula F, Campello-Gómez I, PFR O, Rodríguez-Reinoso F, Martínez-Escandell M, Silvestre-Albero J (2019) Structural flexibility in activated carbon materials prepared under harsh activation conditions. *Materials* 12:1988
- Huang K-J, Zhang J-Z, Shi G-W, Liu Y-M (2014) Hydrothermal synthesis of molybdenum disulfide nanosheets as supercapacitors electrode material. *Electrochim Acta* 132:397–403
- Karaman C (2021) Orange peel derived-nitrogen and sulfur Co-doped carbon dots: a nano-booster for enhancing ORR electrocatalytic performance of 3D graphene networks. *Electroanalysis* 33:1356–1369
- Karaman C, Bayram E, Karaman O, Aktaş Z (2020) Preparation of high surface area nitrogen doped graphene for the assessment of morphologic properties and nitrogen content impacts on supercapacitors. *J Electroanal Chem* 868:114197
- Karaman C, Karaman O, Atar N, Yola ML (2021) Tailoring of cobalt phosphide anchored nitrogen and sulfur co-doped three dimensional graphene hybrid: boosted electrocatalytic performance towards hydrogen evolution reaction. *Electrochim Acta* 380:138262
- Kayani ZN, Butt MZ, Riaz S, Naseem S (2018) Synthesis of NiO nanoparticles by sol-gel technique. *Mater Sci-Pol* 36:547–552
- Kötz R, Carlen M (2000) Principles and applications of electrochemical capacitors. *Electrochim Acta* 45:2483–2498
- Kumar A, Dixit CK (2017) Methods for characterization of nanoparticles, *Advances in nanomedicine for the delivery of therapeutic nucleic acids*. Elsevier, pp:43–58
- Lamiel C, Kumar DR, Shim J-J (2017) Microwave-assisted binder-free synthesis of 3D Ni-Co-Mn oxide nanoflakes@ Ni foam electrode for supercapacitor applications. *Chem Eng J* 316:1091–1102
- Lashkenari MS, Ghorbani M, Silakhori N, Karimi-Maleh H (2021) Enhanced electrochemical performance and stability of Pt/Ni electrocatalyst supported on SiO₂-PANI nanocomposite: a combined experimental and theoretical study. *Mater Chem Phys* 262: 124290
- Lee JW, Hall AS, Kim J-D, Mallouk TE (2012a) A facile and template-free hydrothermal synthesis of Mn₃O₄ nanorods on graphene sheets for supercapacitor electrodes with long cycle stability. *Chem Mater* 24:1158–1164
- Lee JW, Ko JM, Kim J-D (2012b) Hydrothermal preparation of nitrogen-doped graphene sheets via hexamethylenetetramine for application as supercapacitor electrodes. *Electrochim Acta* 85:459–466
- Lota K, Sierczynska A, Lota G (2011) Supercapacitors based on nickel oxide/carbon materials composites. *International Journal of Electrochemistry* 2011:1–6
- Lu Q, Lattanzi MW, Chen Y, Kou X, Li W, Fan X, Unruh KM, Chen JG, Xiao JQ (2011) Supercapacitor electrodes with high-energy and power densities prepared from monolithic NiO/Ni nanocomposites. *Angew Chem Int Ed* 50:6847–6850
- Miller JR, Simon P (2008) Electrochemical capacitors for energy management. *Science Magazine* 321:651–652
- Mopoung S, Moonsri P, Palas W (2015) Khumpai S (2015): Characterization and properties of activated carbon prepared from tamarind seeds by KOH activation for Fe (III) adsorption from aqueous solution. *Sci World J* 2015:1–9
- Moradlou O, Ansarinejad H, Hosseinzadeh M, Kazemi H (2018) High-performance solid state asymmetric supercapacitor based on electrochemically decorated 3D network-like Co₃O₄ architecture on NiO nanoworms. *J Alloys Compd* 755:231–241
- Nyholm L, Nyström G, Mihranyan A, Stromme M (2011) Toward flexible polymer and paper-based energy storage devices. *Adv Mater* 23:3751–3769
- Saidur R, Abdelaziz E, Demirbas A, Hossain M, Mekhilef S (2011) A review on biomass as a fuel for boilers. *Renew Sust Energ Rev* 15: 2262–2289
- Service RF (2006) New ‘supercapacitor’ promises to pack more electrical punch. *American Association for the Advancement of Science*
- Shalan AE, Sharmoukh W, Elshazly AN, Elnagar MM, Al Kiey SA, Rashad MM, Allam NK (2020) Dopant-free hole-transporting polymers for efficient, stable, and hysteresis-less perovskite solar cells. *Sustain Mater Technol* 26:e00226
- Sharmoukh W, Al Kiey SA, Ali BA, Menon L, Allam NK (2020) Recent progress in the development of hole-transport materials to boost the power conversion efficiency of perovskite solar cells. *Sustainable Materials and Technologies*, e00210
- Simon P, Gogotsi Y (2010) Materials for electrochemical capacitors, *Nanoscience and technology: a collection of reviews from Nature journals*. World Scientific, pp:320–329

- Subramanian V, Luo C, Stephan AM, Nahm K, Thomas S, Wei B (2007) Supercapacitors from activated carbon derived from banana fibers. *J Phys Chem C* 111:7527–7531
- Thomas P, Lai CW, Johan MRB (2019) Recent developments in biomass-derived carbon as a potential sustainable material for super-capacitor-based energy storage and environmental applications. *J Anal Appl Pyrolysis* 140:54–85
- Thommes M, Kaneko K, Neimark AV, Olivier JP, Rodriguez-Reinoso F, Rouquerol J, Sing KS (2015) Physisorption of gases, with special reference to the evaluation of surface area and pore size distribution (IUPAC Technical Report). *Pure Appl Chem* 87:1051–1069
- Wang H, Zhong Y, Li Q, Yang J, Dai Q (2008) Cationic starch as a precursor to prepare porous activated carbon for application in supercapacitor electrodes. *J Phys Chem Solids* 69:2420–2425
- Wang G, Zhang L, Zhang J (2012) A review of electrode materials for electrochemical supercapacitors. *Chem Soc Rev* 41:797–828
- Wang C, Xu J, Yuen MF, Zhang J, Li Y, Chen X, Zhang W (2014) Hierarchical composite electrodes of nickel oxide nanoflake 3D graphene for high-performance pseudocapacitors. *Adv Funct Mater* 24:6372–6380
- Wang Y, Guo J, Wang T, Shao J, Wang D, Yang Y-W (2015) Mesoporous transition metal oxides for supercapacitors. *Nanomaterials* 5:1667–1689
- Warren R, Sammoura F, Tounsi F, Sanghadasa M, Lin L (2015) Highly active ruthenium oxide coating via ALD and electrochemical activation in supercapacitor applications. *J Mater Chem A* 3:15568–15575
- Wei L, Yushin G (2012) Nanostructured activated carbons from natural precursors for electrical double layer capacitors. *Nano Energy* 1: 552–565
- Wei W, Cui X, Chen W, Ivey DG (2011) Manganese oxide-based materials as electrochemical supercapacitor electrodes. *Chem Soc Rev* 40:1697–1721
- Wu ZS, Wang DW, Ren W, Zhao J, Zhou G, Li F, Cheng HM (2010) Anchoring hydrous RuO₂ on graphene sheets for high-performance electrochemical capacitors. *Adv Funct Mater* 20:3595–3602
- Zeng Y, Yu M, Meng Y, Fang P, Lu X, Tong Y (2016) Iron-based supercapacitor electrodes: advances and challenges. *Adv Energy Mater* 6:1601053
- Zhao S, Wang C-Y, Chen M-M, Wang J, Shi Z-Q (2009) Potato starch-based activated carbon spheres as electrode material for electrochemical capacitor. *J Phys Chem Solids* 70:1256–1260

Publisher's note Springer Nature remains neutral with regard to jurisdictional claims in published maps and institutional affiliations.